

## Kelvin-Helmholtz modes revealed by the transversal structure of the jet in 0836+710.

M. Perucho and A. P. Lobanov

*Max-Planck-Institut für Radioastronomie, Auf dem Hügel, 69, 53121, Bonn, Germany.*

**Abstract.** Studying transversal structure in extragalactic jets is crucial for understanding their physics. The Japanese led space VLBI project VSOP has offered arguably the best opportunity for such studies, by reaching baseline lengths of up to 36,000 km and resolving structures down to an angular size of 0.3 mas at 5 GHz. VSOP observations of the jet in 0836+710 at 1.6 and 5 GHz have enabled tracing the radial structure of the flow on scales from 2 mas to 200 mas and determining the wavelengths of individual oscillatory modes responsible for the formation of the structure observed. We conclude that these modes are produced by Kelvin-Helmholtz instability in a sheared relativistic flow. Our results point towards the stratification of the jet and the growth of different modes at different jet radii. We also discuss the implications of the driving frequency on the physics of the active nucleus of the quasar.

### 1. Introduction

Resolving the transversal (or radial) structure in extragalactic jets is a crucial step in our understanding of the physics of these objects. On parsec scales, this has become feasible only recently, using space VLBI<sup>1</sup> observations with the VSOP<sup>2</sup> (Lobanov & Zensus 2001). These observations revealed the presence of a double helical structure inside the jet of 3C 273, which can be attributed to a combination of the helical and elliptic modes of Kelvin-Helmholtz (KH) instability. Numerical simulations further support this interpretation (Perucho et al. 2006). We report here on further progress of this investigation. We use VSOP observations of the radio jet in the quasar S5 0836+710 at 1.6 and 5 GHz to estimate basic physical properties of the relativistic flow, focusing specifically on the radial profiles of its velocity and density.

The luminous quasar S5 0836+710 at a redshift  $z = 2.16$  hosts a powerful radio jet extending up to kiloparsec scales (Hummel et al. 1992). VLBI monitoring of the source (Otterbein et al. 1998) has yielded estimates of the bulk Lorentz factor  $\gamma_j = 12$  and the viewing angle  $\theta_j = 3^\circ$  of the flow. Presence of an instability developing in the jet is suggested by the kink structures observed on milliarcsecond scales with ground VLBI (Krichbaum et al. 1990).

In the VSOP image of 0836+710 at 5 GHz, oscillations of the jet ridge line are observed (Lobanov et al. 1998), with a wavelength of 7.7 mas. In addition

---

<sup>1</sup>Very Long Baseline Interferometry

<sup>2</sup>VLBI Space Observatory Programme

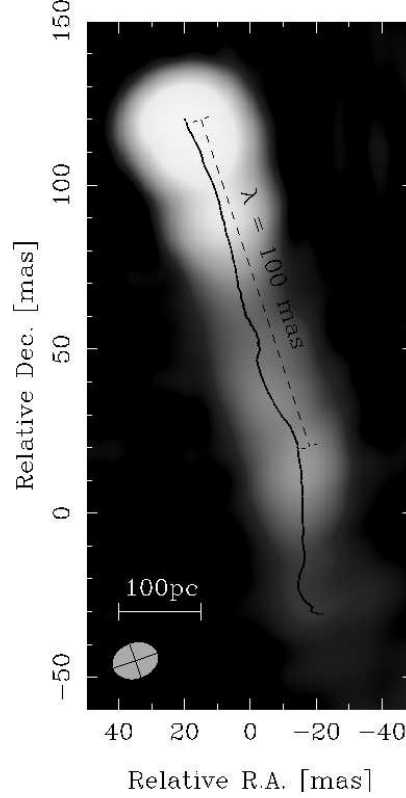


Figure 1. 1.6 GHz image of the jet in 0836+710. The ridge line of the jet is overprinted and the 100 mas mode is identified.

to this, a 4.6 mas periodicity is found in the spectral index distribution. Using the vortex sheet approximation (Hardee 2000), these structures have been identified with the helical surface and elliptic surface modes of KH instability, yielding estimates of basic physical properties of the flow: the Lorentz factor  $\gamma_j \sim 11$ , Mach number  $M_j \sim 6$  and jet/ambient medium density ratio  $\eta(\rho_j/\rho_a) = 0.04$ . High dynamic range VLBA<sup>3</sup> observations of 0836+710 at 1.6 GHz show the presence of an oscillation at a wavelength as long as  $\sim 100$  mas (Lobanov et al. 2006). Fig. 1 shows a 1.6 GHz image of the jet with the ridge line of the emission overprinted. The image also shows the identification of the 100 mas wave. This wavelength cannot be readily reconciled with the jet parameters determined from the two shorter wavelength oscillations, indicating that the flow may have a complex, stratified transversal structure in which emission at lower frequencies originates from outer layers of the flow.

There are two basic explanations for the fact that the longest wavelength does not fit within the scenario described above: 1) the jet parameters derived may not be exact, or 2) the approximations and assumptions used in the KH

---

<sup>3</sup>Very Long Baseline Array of National Radio Astronomy Observatory, USA

linear theory are not strictly valid. In this work we use the parameters derived in Otterbein et al. (1998) from the spectral evolution in the jet, and relax the approximation to vortex sheet contact discontinuity between the jet and the ambient medium, used in the stability analysis in Lobanov et al. (1998), exploring the possibility of the jet being sheared.

We show that the presence of a shear layer allows to fit all the observed wavelengths within a single set of parameters, assuming that they are produced due to KH instabilities growing in a cylindrical outflow. In this picture, the longest mode corresponds to a surface mode growing in the outer layers, whereas the shorter wavelengths are identified with body modes developing in the inner radii of the jet.

In Section 2, we describe the method used to solve the linear stability problem for cylindric relativistic flows and provide the respective solutions for the set of parameters given in Lobanov et al. (1998). These solutions are compared in Section 3 with the wavelengths observed in the jet of 0836+710. Section 4 summarizes the main results of this work and puts them in the broader context of the physics of relativistic outflows.

## 2. Linear Analysis

We describe the flow in cylindrical coordinates  $(r, z, \phi)$ , with  $r$  and  $z$  defining the radial and axial directions, respectively. We consider a sheared transition in the axial velocity,  $v_z$  and the rest mass density,  $\rho$ , between the jet and the ambient medium of the following form (see Perucho et al. 2007 for a detailed description of the linear analysis)  $a(r) = a_\infty + (a_0 - a_\infty) / \cosh(r^m)$ , where  $a(x)$  is the profiled quantity ( $v_z$  or  $\rho$ ) and  $a_0, a_\infty$  are its values at the jet symmetry plane (at  $r = 0$ ) and at  $r \rightarrow \infty$ , respectively. The integer  $m$  controls the steepness of the shear layer. In the limit  $m \rightarrow \infty$ , the configuration turns into the vortex-sheet case, as described by Hardee (2000). The jet and the ambient medium are in pressure equilibrium. An adiabatic perturbation of the form  $\propto g(r) \exp[i(k_z z - \omega t)]$  is introduced in the equations of the flow<sup>4</sup>, where  $\omega$  and  $k_z$  are the frequency and longitudinal wavenumber of the perturbation, respectively, and the function  $g(r)$  defines the radial structure of the perturbation. The units used are the jet radius,  $R_j$ , and the speed of light,  $c$ . After some algebra, we obtain the following second order differential equation for the pressure perturbation (equation 13 in Birkinshaw 1984):

$$P_1'' + \left( \frac{2\gamma_0^2 v_{0z}' (k_z - \omega v_{0z})}{\omega - v_{0z} k_z} - \frac{\rho_{e,0}'}{\rho_{e,0} + P_0} \right) P_1' + \gamma_0^2 \left( \frac{(\omega - v_{0z} k_z)^2}{c_{s,0}^2} - (k_z - \omega v_{0z})^2 \right) P_1 = 0. \quad (1)$$

Equation 1 is solved by applying the *shooting method* (Press et al. 1997). This method requires integration of the equation from the jet axis to a point outside the jet. We impose boundary conditions on the amplitude of the pressure

---

<sup>4</sup>We assume that the magnetic field is not dynamically important.

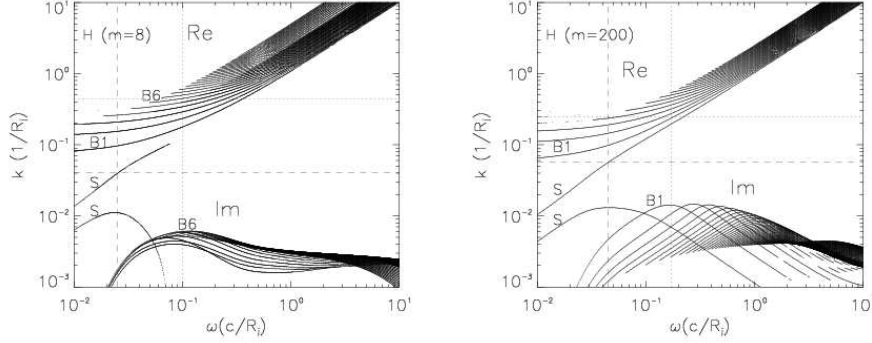


Figure 2. Real (upper curves in each plot) and imaginary (lower curves in each plot) parts of the wavenumber versus frequency for the helical modes and the parameters given for the jet in 0836+710. The upper panel shows the solutions for  $m = 8$  and the lower plot shows the solutions for  $m = 200$ . The vertical dashed lines indicate the minimum growth lengths of the surface modes, whereas the vertical dotted lines indicate the minimum growth length of the first body modes for  $m = 200$  and the minimum growth length of all body modes for  $m = 8$ . The horizontal lines indicate the wave number at which the minimum growth length occurs.  $S$  stands for the surface mode,  $B1$  for the first body mode, and  $B5$ - $B6$  indicate the body mode that gives the minimum growth lengths for  $m = 8$ .

perturbation and on its first derivative on the jet axis, depending on the symmetry or antisymmetry of the perturbation on the jet axis. Then, for a given frequency ( $\omega$ ), a complex wavenumber is given. The integration is done using a variable-step Runge-Kutta method (Press et al. 1997). When the integration reaches the given point outside the jet, the value obtained is compared with the boundary conditions there: The Sommerfeld condition, requiring the solutions to approach zero at infinity, and the requirement of no incoming waves at infinity. These conditions ensure that the solutions can be given by Bessel functions inside the jet and Hankel functions outside. Appropriate values of the complex wavenumber that fit into those conditions are searched using the Müller method (Press et al. 1997). As stated above, the solutions are obtained in the spatial domain, i.e., assuming  $\omega$  is real and  $k$  is complex. In this description, the inverse of the imaginary part of the wavenumber,  $1/\text{Im}(k)$ , gives the growth length (or  $e$ -folding length), defined as the distance at which the perturbation amplitude increases by one exponential factor. We adopt the jet parameters derived in Otterbein et al. (1998); Lobanov et al. (1998, 2006) and solve the pressure perturbation equation with several different values of  $m$ . The resulting solutions are plotted in Fig. 2 for the helical instability modes and for two values of  $m$ :  $m = 8$  (left panels) and  $m = 200$  (right panels). The  $m = 8$  case corresponds to a broad shear layer of  $\sim 0.6 R_j$  in width, whereas the  $m = 200$  one implies a shear layer width of  $\sim 0.1 R_j$ , i.e., approaching the vortex-sheet case.

The plots in Fig. 2 indicate that, in thicker shear layers ( $m = 8$ ), the surface mode grows faster than the body modes. The minimum growth lengths (maximum  $k_{im}$ ) of the surface mode, indicated by vertical dashed lines in Fig. 2, are realized at long wavelengths (horizontal dashed lines show the wavenumber

of the mode):  $\lambda_{S,H,8}^* \sim 160 R_j$ , at  $\omega = 0.025 c/R_j$ . The smallest growth lengths of all body modes are achieved by the fifth and sixth order body modes at  $\lambda_{B6,8} \sim 14 R_j$ .

For a thin shear layer ( $m = 200$ ) the minimum growth lengths of low order helical body modes are similar to that of the helical surface mode, with the minimum realized for the first body mode at  $\lambda_{B1,200} \sim 25 R_j$ . The minimum growth length of the surface modes shifts to higher frequencies and shorter wavelengths ( $\lambda_{S,H,200}^* \sim 100 R_j$ ) compared to the respective values obtained for  $m = 8$ . For  $m < 8$ , the growths of all the modes are strongly reduced as the width of the shear layer is increased. For  $m > 200$  the solutions converge to the vortex-sheet case also at the highest frequencies/shortest wavelengths.

### 3. Results: From Theory to Observations

The solutions of the linear stability problem obtained in the previous section can be compared with the wavelengths observed in the jet in 0836+710. This comparison requires an estimate of the radius of the jet, in order to convert the frequencies and wavenumbers of the solution into physical units. The true jet radius can be estimated from the VLBA radio maps presented in Lobanov et al. (1998, 2006), using the following relation:  $R_j(\text{mas}) = 0.5(D_i^2 - b^2)^{1/2}$ , where  $D_i$  is the observed width of the jet and  $b$  is the beam width transversally to the direction of the jet. We measure the diameter of the jet and the beamwidth at 1% of the peak emission (Wehrle et al. 1992) at the base of the jet, implicitly assuming that the outer parts of the shear layer emit less than 1% of the radio power at these frequencies. This yields the jet radii of  $R_{j,1.6} \sim 17 \text{ mas}$  and  $R_{j,5} \sim 0.64 \text{ mas}$  at 1.6 GHz and 5 GHz, respectively. If the jet is assumed to be sheared, the radius we need to consider is that at 1.6 GHz, as it includes the outer, slower layers of the jet. Thus, taking the radius of the jet to be  $R_j \sim 17 \text{ mas}$ , the 100 mas structure turns into  $\lambda \sim 6 R_j$ , and the 7.7 mas into  $\lambda \sim 0.2 R_j$ .

The intrinsic (rest frame) wavelengths derived from the solutions to Eq. 1 shown in Fig. 2,  $\lambda_{\text{int}}$ , can then be transformed to the observer's frame and expressed also in units of  $R_j$ . The observed wavelengths are obtained by adding the corrections for relativistic motion, projection and cosmological effects through the following relation:

$$\lambda_{\text{obs}} = \frac{\lambda_{\text{int}} \sin \theta_j}{(1+z)(1-v_w/c \cos \theta_j)}, \quad (2)$$

where  $\lambda_{\text{obs}}$  is the observed wavelength,  $z$  is the redshift,  $v_w$  is the wave speed and  $\theta_j$  is the jet angle to the line of sight. The wave speed  $v_w = \omega/k$  is obtained from the solutions to the linear problem (Fig. 2).

We focus first in the helical surface mode, most likely responsible for the longest observed wavelength of 100 mas. The wave speed of the helical surface mode ranges from  $v_w \sim 0.6 c$  to  $v_w \sim 0.8 c$ , for the thicker and thinner shear-layer, respectively. We obtain, in the case of the thick shear layer, a wavelength of  $6.6 R_j$ , whereas in the case of a thin shear layer we obtain  $8.2 R_j$ .

For the case of the body modes, visible at 5 GHz, we find a wave speed of  $v_w \sim 0.2 c$  for the fifth and sixth body modes (those with the fastest growths) in

the case of a thick shear layer, and a wave speed of  $v_w \sim 0.7c$  for the first body mode in the case of a thin shear layer. These modes would produce structure with an observed wavelengths of  $0.29 R_j$  and  $1.4 R_j$ , respectively.

The wavelengths obtained for the thick shear layer are close to those observed:  $6.6 R_j$  from theory compared to  $6 R_j$  from the observations for the longest structure and  $0.29 R_j$  from theory compared to  $0.2 R_j$  from the observations. This agreement is also remarkable in the case of the 4.6 mas structure, identified in Lobanov et al. (2006) as an elliptic mode and not discussed here. This leads us to conclude that the jet is transversally stratified (i.e., has a thick shear layer), although the lack of error estimates precludes us from ruling out firmly the scenario with a thin shear layer.

#### 4. Discussion

The description developed in this work explains all three major oscillations observed in the jet of 0836+710, if the flow speed and density are both transversely stratified. The longest observed wavelength of 100 mas represents the helical surface mode, whereas the two shorter ones (7.7 mas and 4.6 mas) are identified with the fifth/sixth order helical and elliptic body modes, respectively. The former is observed in the images of the jet at 1.6 GHz (see Fig. 1) and the latter are observed at 5 GHz. The whole picture fits into the theory if the radius of the jet at the lowest observed frequency is taken, implying that the body modes have their maxima at inner regions of the jet than the surface mode. If we take the radius of the jet at 5 GHz, the short observed wavelengths may be interpreted as surface modes and the longest mode cannot, in that case, be explained by KH theory (Lobanov et al. 2006). A second implication of this result is that the radiating particles emitting at 5 GHz occupy a central spine in a stratified jet, while the longer-wavelength structure seen at 1.6 GHz is generated in outer layers of the flow.

One possible alternative to the stratified jet scenario is to consider deviations of the basic jet parameters from those derived in Lobanov et al. (1998, 2006). To assess this alternative, we have calculated the solutions of the stability equation for different sets of parameters, varying the jet Lorentz factor, rest-mass density ratio and specific internal energy. We conclude that the jet in 0836+710 must have (on axis) a Lorentz factor close to 12 or slightly smaller, a density ratio of  $10^{-2}$ – $10^{-1}$  and a sound speed  $c_{s,j} \sim 0.2$  or slightly larger — not deviating much from the parameters derived in Otterbein et al. (1998); Lobanov et al. (1998, 2006), which supports the conclusions derived in this paper.

Further work in the stability analysis would focus on solving the differential equation for the pressure perturbation (Eq. 1) using a relativistic equation of state that allows for inclusion of different families of particles. This will enable testing the solutions for a proton-electron jet and an electron-positron jet, providing an useful insight into the jet composition.

It has been shown by Hardee et al. (1994) that the helical surface mode of KH instability can be driven by an external periodic process. In this case, coupling this process to the helical surface mode requires the driving frequency to be lower than the resonant frequency. For 0836+710, the driving frequency of the helical surface mode at its minimum growth length is  $0.025 c/R_j$  would

imply a driving period of  $T_{\text{dr}} \sim 5.6 \cdot 10^7$  yrs. This is similar to the driving period of  $\sim 2 \cdot 10^7$  yrs found for 3C 449 (Hardee et al. 1994). Periodic variations of the jet ejection axis can be produced by a number of physical processes, including a binary black hole and a misaligned torus as the most plausible (Appl et al. 1996). However, a misaligned torus can only produced a period of  $10^3 - 10^5$  yrs, depending on the accretion disk and black-hole properties (Lu & Zhou 2005) in the case of 0836+710 (Perucho & Lobanov (2007b)). On the other hand, if we combine the value derived for  $T_{\text{dr}}$  with the estimate of the black hole mass in 0836+710 ( $2 \cdot 10^8 - 10^9 M_{\odot}$ ; Tavecchio et al. 2000), we obtain a companion mass of  $10^4 - 10^7 M_{\odot}$ , depending on the separation between the two black holes ( $10^{17} - 10^{18}$  cm). The latter is thus a possible explanation for the precession period obtained from our analysis.

Finally, the kiloparsec-scale structure of 0836+710 shows a large, decollimated feature (Hummel et al. 1992), without any emission between it and the 1.6 GHz jet. New observations with high dynamic range that have already been performed will give us more insight into the properties of this jet on the kiloparsec scales and could show whether the cause of the decollimation on the kiloparsec scales is the disruption of the jet by the 100 mas structure, identified here as a helical surface mode.

**Acknowledgments.** This work was supported in part by the Spanish Dirección General de Enseñanza Superior under grants AYA-2001-3490-C02 and AYA2004-08067-C03-01. M.P. is supported by a postdoctoral fellowship of the Generalitat Valenciana (*Beca Postdoctoral d'Excel·lència*).

## References

- Appl, S., Sol, H., Vicente, L. 1996, A&A, 310, 419  
 Birkinshaw, M. 1984 MNRAS, 208, 887  
 Caccianiga, A., Marcha, M.J., Antón, S., Mack, K.H., Neeser, M.J. 2002, MNRAS, 329, 877  
 Hardee, P.E., Cooper, M.A., Clarke, D.A. 1994, ApJ, 424, 126  
 Hardee, P.E. 2000, ApJ, 533, 176  
 Krichbaum, T.P., Hummel, C.A., Quirrenbach, A., et al. 1990, A&A, 230, 271  
 Lobanov, A.P., Krichbaum, T.P., Witzel, A., et al. 1998, A&A, 340, 60  
 Lobanov, A.P., and Zensus, J.A. 2001, Science, 294, 128  
 Lobanov, A.P., Krichbaum, T.P., Witzel, A., Zensus, J.A. 2006, PASJ, 58, 253  
 Lu, J.F., Zhou, B.Y. 2005, ApJL, 635, 17  
 Hummel, C.A., Muxlow, T.W.B., Krichbaum, T.P., et al. 1992, A&A, 266, 93  
 Otterbein, K., Krichbaum, T.P., Kraus, A., et al. 1998, A&A, 334, 489  
 Perucho, M., Lobanov, A.P., Martí, J.M., Hardee, P.E. 2006, A&A, 456, 493  
 Perucho, M., and Lobanov, A.P. 2007, proceedings of *Primer Encuentro de la Radioastronomía Española*, eds. J.C. Guirado, I. Martí and J.M. Marcaide, in press (astro-ph/0607386)  
 Perucho, M., Hanasz, M., Martí, J.M., and Miralles, J.A. 2007, Phy. Rev. E, 75e6312  
 Perucho, M., and Lobanov, A.P. 2007, A&A Letters, 469, 23  
 Press, W.H., Teukolsky, S.A., Vetterling, W.T., Flannery, B.P. *Numerical recipes*, Cambridge Univ. Press 1997  
 Tavecchio, F., Maraschi, L., Ghisellini, G., et al. 2000, ApJ, 543, 535  
 Wehrle, A.E., Cohen, M.H., Unwin, S.C., Aller, H.D., Aller, M.F., Nicolson, G. 1992, ApJ, 391, 589